Thermochimica Acta 588 (2014) 1–10

Contents lists available at ScienceDirect

Thermochimica Acta

journal homepage: www.elsevier.com/locate/tca

Short Communication

Estimation of the thermal properties of hardened cement paste on the basis of guarded heat flow meter measurements

Seyoon Yoon, Donald E. Macphee, Mohammed S. Imbabi*

School of Engineering, Kings College, University of Aberdeen, Aberdeen AB9 2UE, UK

ARTICLE INFO

Article history:
Received 5 July 2013
Received in revised form 1 April 2014
Accepted 15 April 2014
Available online 23 April 2014

Keywords:
Cement
Concrete
Thermal conductivity
Thermal diffusivity
Specific heat capacity
Heat flow meter

ABSTRACT

In the present study, a new analysis method is proposed to measure thermal conductivity, thermal diffusivity, volumetric specific heat capacity, and specific heat capacity of cement-based materials based on the guarded heat flow meter apparatus. We tested hydrated cement paste specimens with 0.4 water-to-cement ratio and applied both steady and non-steady state data to compute thermal properties of the hydrated cement paste. Thermal conductivity and thermal contact resistance were determined as $1.28\,W\,m^{-1}\,K^{-1}$ and $0.038\,m^{-2}\,K\,W^{-1}$ using steady state data. Furthermore, using a computerized system of heat flow meters and non-linear regression, we used non-steady state data to measure thermal diffusivity, volumetric specific heat capacity and specific heat capacity of the hydrated cement paste as $4.77 \times 10^{-7}\,m^2\,s^{-1}$, $2685.4\,kJ\,m^{-3}\,K^{-1}$, and $1.28\,kJ\,kg^{-1}\,K^{-1}$. The relative uncertainties of these properties fell within 2–7% range and the residual distributions were validated to follow a normal distribution based on quantile–quantile tests.

1. Introduction

The need for improved thermal insulation properties and accurate evaluation of the effects of heat-transfer on energy use and carbon emissions in buildings and structures is widely acknowledged within the engineering community. Good thermal insulation is essential if we are to meet the demands of energy efficiency and decent indoor thermal comfort that are required to achieve a low energy, low carbon and sustainable way of life in future. There are many other applications where good thermal insulation is required to conserve heat or reduce thermal loading on a structure, for example the refractory lining of a rotary kiln in Portland cement clinker production or the radiation shield of a nuclear power plant.

The three key properties that are required in the study of the thermal insulating properties and heat transfer through materials are thermal conductivity, specific heat capacity and thermal diffusivity [1]. Thermal conductivity is a measure of a material's ability to transmit heat by conduction and is one of the basic parameters used to determine properties such as the thermal resistance (*R*-value) or alternatively the overall heat transfer coefficient (*U*-value) of the external envelope (or envelope element) of a building. Specific heat capacity, on the other hand, describes the capacity of the material to absorb, store and release heat. It is widely used in thermodynamic analysis and in Dynamic Simulation Modeling of buildings, to simulate inertial effects and predict heating profiles and annual energy demand. Lastly, thermal diffusivity is the parameter that defines the transient thermal profile during unsteady, transition periods in the heating/cooling cycle. It is the parameter that links thermal conductivity and specific heat capacity.

Cements, and cement products such as concrete, are amongst the most commonly used construction materials in the world. Knowing their thermal properties is important if we are to meet the sustainability challenges that we face. There are two generic approaches to measuring the thermal conductivity of materials: steady state tests and non-steady state tests [2]. The Radial Heat Flow (RHF), Guarded Hot Plate (GHP), and Guarded Heat Flow Meter (GHFM) methods are steady state tests, and the Hot Wire (HW) and Transient Plane Source (TPS) methods are non-steady state tests. The thermal properties of cementitious materials have been tested using these methods. Bentz [3], Bouguerra et al. [4], and Milovanovic et al. [5] used TPS for hydrated cement pastes, Kim et al. [6] applied the Two-Linear-Parallel-Probe (TLPP) method to hydrated cement paste and concrete, and Khan [7] and Mounanga et al. [8] used the HW method for hydrated cement and concrete. Other researchers have applied these test methods to other cementitious materials, such as lightweight concrete and geopolymers [9,10]. Furthermore, Fokaides et al. recently applied infrared thermography to measure the *U*-value of building envelopes [11]. The reported values for thermal conductivity of hydrated cement pastes, at water-to-cement (w/c) ratio of

* Corresponding author. Tel.: +44 1224 272506; fax: +44 1224 272497.
E-mail address: m.s.imbabi@abdn.ac.uk (M.S. Imbabi).

http://dx.doi.org/10.1016/j.tca.2014.04.015
0040-6031/

Table 1
Literature values for the thermal conductivity of comparable hydrated cement pastes.

Author	Method	Specimen description	Surface condition	Temperature (°C)	Conductivity ($W m^{-1} K^{-1}$)
Kim et al. [7]	Two-linear-parallel-probe	Hydrated cement paste in saturation (w/c = 0.4)	Flat cast	20 and 40	1.16 and 1.13
Bentz [3]	Transient plane source	Hydrated cement paste in saturation (w/c = 0.4)	Flat cast	23	0.94
Milovanovic et al. [5]	Transient plane source	Hydrated cement paste in saturation (w/c = 0.4)	Flat cast	20	1.81
Bouguerra et al. [4]	Transient plane source	Hydrated cement paste in saturation (density = 2100 kg/m^3)	Crushed	20	2.85

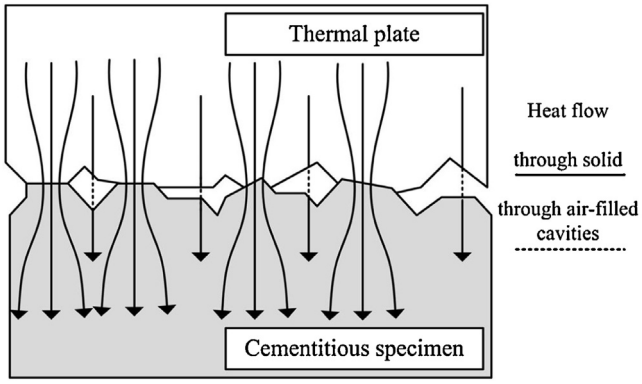

Fig. 1. Illustration of heat flow between instrument and specimen.

0.4, measured under saturated condition, are summarized in Table 1. According to Kim et al. [6], the difference in the thermal conductivity between hardened cement pastes with 0.25 and 0.4 water-to-cement ratios was only 0.058 $W m^{-1} K^{-1}$. Notwithstanding the compositional uncertainty and complexity of cementitious materials, the differences between the values reported are high by any stretch of the imagination and are therefore probably subject to unquantified experimental artifacts as the relevant literature refers to equivalent mix proportioning and similar test conditions.

The purpose of the work reported in this paper is to investigate and understand the reason(s) for these large variations and anomalies, and to develop a consistent analysis method for determining the thermal conductivity and other thermal properties of cementitious materials. In common, the large scatter in measured values of thermal conductivity is developed by the contact resistance between the test apparatus and the sample. Martias et al. took into account the contact resistance to measure the thermal conductivities of gypsum composites [12]. Contact resistance is the interfacial thermal resistance between the specimen surface and the heat flow meter as illustrated in Fig. 1 [13]. As shown in Table 1, crushed cement pastes having rough surface characteristics show very different thermal conductivities compared to other samples because of relative differences in their surface profiles. Because the proportions between porosity and cement matrix play a strong role in determining the density of hardened cement pastes, the identical w/c ratio provides similar density. In the present study, the density of the samples with 0.4 w/c ratio is 2086 $kg m^{-3}$, which is similar to crushed cement pastes (2100 $kg m^{-3}$). Furthermore, since other data listed in Table 1 has been obtained for hardened cement pastes with 0.4 w/c ratio, the thermal conductivities in Table 1 will be comparable to the results measured by the present study.

The contact resistance is of relevance in almost all measurement techniques, apart from non-contact methods such as the laser flash method [14,15]. The hardened cement paste is a complex porous material that contains both a persistent solid matrix and a void space, of which the dimensional range is from nano-to-millimeters in size [16]. The wide range of pore sizes in a hydrated cement paste provides "inhomogeneous and complex" surface characteristics. For dense cementitious materials, therefore, the effect of contact resistance is severe as they present relatively high thermal conductivities compared to insulation materials and generally rough, non-compliant surfaces. In the present study we present evidence of the significant effect of contact resistance on thermal conductivity measurement tests of cementitious materials. We also introduce a new computational method in which measured experimental data are first compared with outputs from a mathematical model of thermal conductivity in which the effect of contact resistance has been explicitly included. Using this model, we then show how the value of the contact resistance for the sample of material being tested can be calculated to allow the thermal conductivity and other thermal properties of the material to be described. An extension of the new computational method has been developed to enable the use of non-steady state (transient) data from the guarded heat flow meter test to also determine the specific heat capacity and thermal diffusivity. This is a meaningful departure from the traditional steady-state only use of the guarded heat flow meter test. Our proposed unified method for consistent, simultaneous measurement of the thermal conductivity, specific heat capacity and thermal diffusivity of cementitious (and other dense) materials significantly improves the utility of the guarded heat flow meter method. With the "Guide to the Expression of Uncertainty in Measurement" (GUM) [17], the expression of uncertainty provides a uniform basis for the comparison of experimental results and methods. This guide was therefore used for the determination of the standard and relative uncertainties of measured thermal properties.

2. Description of guarded heat flow meter apparatus

The guarded heat flow meter apparatus and guarded hot plate are routinely used worldwide for testing thermal conductivity, and many standard test methods are based on these apparatuses [20–22]. The two methods are similar in terms of mathematical theory and apparatus configuration. Their difference is that the guarded heat flow meter determines the density of heat flow relative to the reference material while the guarded hot plate is a direct measurement of the generated heat flow. Furthermore, a modified apparatus based on similar principles, the guarded parallel-plate instrument, has also been used for the thermal conductivity of fluids [23].

A more uniform surface profile can reduce the measurement uncertainty of contact resistance. In order to generate the uniform surface profile, the sample surfaces, however, need to be treated or polished, meaning that a smaller contact area has a practical advantage in terms of effort expended in sample preparation. The guarded heat flow meter apparatus generates one-dimensional heat flow through a test specimen that is firmly sandwiched

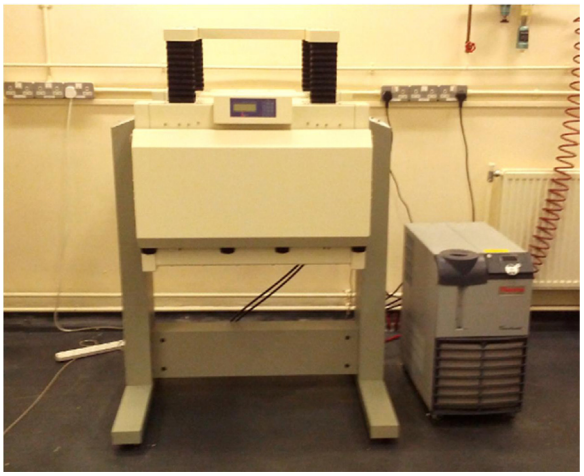

Fig. 2. FOX-603 thermal conductivity test apparatus.

between two parallel plates maintained at constant but different temperatures. The specimen is contained between the isothermal plates and the density of heat flow is measured by the heat flow meters. It is important to confirm that the isothermal plates reach the desired temperatures by mounting thermocouples on the isothermal plates. The FOX 600 series of thermal conductivity test machines require no pre-test calibration. The apparatus, shown in Fig. 2, was used in the present study.

3. Mathematical models

The operating principle of the guarded heat flow meter method is to generate a unidirectional heat flow through the test specimen when a temperature difference is applied. The governing differential equation is that of heat conduction in a one-dimensional continuum in which it is assumed that the thermal conductivity of the material is independent of temperature [24]. The total thermal resistance, which is generated by the specimen and contact surfaces, needs to be taken into account. The following model developed by Tleoubaev et al. explicitly includes the contact resistance [25,26]:

$$q_{\text{total}} = SE = \frac{\Delta T}{R_{\text{total}}} = \frac{\Delta T}{\Delta x/\lambda + 2R_{\text{contact}}} \tag{1}$$

where, q_{total} is the measured density of heat flow, S is the calibration constant which is specific for the heat flow meter ($\text{W m}^{-2}\,\mu\text{V}^{-1}$), E is heat flow meters' signal (μV), ΔT is the temperature difference between isothermal plates, Δx is the specimen thickness, λ is the thermal conductivity, R_{total} is the total thermal resistance to heat flow, and R_{contact} is the contact resistance, assumed to be identical at each end of the specimen. With low thermal conductivity ($\Delta x/\lambda \gg 2R_{\text{contact}}$), the reasonable estimates of heat flow can be obtained by ignoring the contact resistance. For cementitious materials, the ratio of the thermal contact resistance to the total thermal resistance is much larger and the thermal contact resistance cannot be neglected.

Tleoubaev et al. measured two samples of different thicknesses to obtain two unknown values, which are the contact resistance and thermal conductivity [26]. However, identical specimens of cementitious materials can have different contact resistances due to their complex pore structure and surface characteristics, as well as the method of production and preparation of the specimen surfaces in contact with the heat flow meter(s). This confirms that two data points are insufficient on their own to determine the thermal conductivity of cementitous materials, and also that the surface characteristics have to be quantitatively controlled for the testing of identical specimens with different thicknesses. In Section 4.2 we will subsequently show how the surface characteristics of all specimens can be quantitatively controlled. The analytical solution of the temperature profiles is expressed as follows [27]:

$$T(x,t) = \left(\frac{\Delta T}{L}x + T_L\right) + \sum_{n=1}^{\infty}\beta_n \sin\left(\frac{n\pi x}{L}\right) e^{-(n\pi/L)^2 at} \tag{2}$$

where

$$\beta_n = \frac{2}{L}\int_0^L \left[T_0 - \left(\frac{\Delta T}{L}v + T_L\right)\right] \sin\left(\frac{n\pi v}{L}\right) dv$$

where, T is the temperature at location x and time t, β_n are eigenvalues, a is the thermal diffusivity, 0 and L are the locations contacting the isothermal plates and the sample, T_0 is the initial temperature, and T_L and T_H are respectively the low and high temperature on the isothermal plates. The density of heat flow through the specimen is obtained by differentiating Eq. (2):

$$q_{\text{specimen}}(x,t) = \lambda\frac{\partial T}{\partial x} = \lambda\left\{\frac{\Delta T}{L} + \sum_{n=1}^{\infty}\beta_n\frac{n\pi}{L}\cos\left(\frac{n\pi x}{L}\right) e^{-(n\pi/L)^2 at}\right\} \tag{3}$$

However, this analytical solution does not describe the effect of contact resistance on the density of heat flow measured by the heat flow meter. In order to include the effect of contact resistance and separate Δx in Eq. (1), a new expression for heat flow can be presented as follows:

$$SE = \frac{\Delta T}{\Delta x/\lambda + 2R_{\text{contact}}} \rightarrow \frac{1}{1/SE - 2R_{\text{contact}}/\Delta T} = \lambda\frac{\Delta T}{\Delta x} \tag{4}$$

As Δx approaches zero, the contact resistance can be related to Eq. (3) as:

$$\lim_{\Delta x\to 0}\left\{\frac{1}{1/SE - 2R_{\text{contact}}/\Delta T}\right\} = \lim_{\Delta x\to 0}\left(\lambda\frac{\Delta T}{\Delta x}\right) \rightarrow \frac{1}{1/SE - 2R_{\text{contact}}/\Delta T} = \lambda\left.\frac{\partial T}{\partial x}\right|_{x=0} = q_{\text{specimen}}(0,t) \tag{5}$$

The theoretical solutions presented in Eqs. (3) and (5) can be used to determine the thermal diffusivity and specific heat capacity of the test sample when the temperature discontinuity at interfaces tends to zero. The analytical solution for the cases of major temperature discontinuity is presented in Appendix A. In Section 5 we will show how non-linear regression with non-steady state data can be used to determine these thermal properties of the sample.

4. The experimental test method used

4.1. Materials tested and sample preparation method

All specimens were prepared using ASTM Type III Portland cement, which is equivalent to ordinary Portland cement with regard to chemical composition but has a higher fineness. ASTM Type III was chosen because of its much more rapid rate of hydration and more stable chemical composition compared to ASTM Type I after 28 days [28]. Cement paste cylinders measuring 100 mm diameter × 200 mm height, were produced using 0.4 w/c ratio and cured in water at 20 °C for 28 days before the tests. The cylinders were cut to different thicknesses at 28 days, and fully saturated specimens were used for the thermal tests. During the thermal tests, the circumferential surface boundaries of the

specimens were wrapped and sealed with polyethylene film, and then snuggly insulated using a pre-cut, pre-shaped rigid expanded polystyrene insulation board (Jablite, UK) with measured thermal conductivity of 0.031 $W\,m^{-1}\,K^{-1}$.

4.2. Test conditions

According to the theory of steady-state heat transfer outlined in Section 3, the contact surface 'smoothness' of all of the specimens to be tested is required to be identical. Many stereological parameters have been considered for surface characterization in the literature [29,30]. Among them, the three parameters commonly used are profile roughness ratio, surface roughness ratio, and fractal dimension [29]. For the sake of simplicity, since our aim is to maintain similar surface characteristics for the specimen-boundary in contact with the heat flow meter (as opposed to establishing their absolute surface characteristics), the profile roughness ratio, which is the easiest and simplest parameter to quantify, was adopted in the present study. For this purpose, the polishing process was controlled to obtain similar profile roughnesses for all of the specimens that were tested. The profile roughness was measured by the microscopic method. In essence, the profile roughness ratios of the contact boundary surfaces of all specimens were obtained by dividing the length of the profile line (L) by the projected length of the profile line (L_0) [29]. The profile images for 10 representative areas of each specimen were registered using a light microscope at a magnification of 5×. The image analysis was carried out using standard functions from the MATLAB Image Processing Toolbox. The ten profile roughness ratios of each specimen were averaged and the polishing process was controlled to keep the averages within 1.10 ± 0.05.

The densities of all specimens were measured, and their values ranged within 2086 ± 41 kg/m^3. All thermal tests were performed using LaserComp's FOX 603 thermal conductivity test machine and the data was collected using WinTherm32 and our control software algorithm. In the tests one of the machines isothermal plates generated the 20 °C temperature boundary and the other generated 10 °C, so the temperature difference between the two plates was maintained at 10 °C; ASTM C 518 [21] recommends that the temperature difference across the specimens is not less than 10 °C. Opting for a larger temperature difference can lead to inaccuracies because the thermal conductivity and specific heat capacity of materials will vary with temperature. The values obtained using the guard heat flow meter method thus represent the effective thermal coefficients that can be usefully applied within the range of the boundary temperatures of the test. There are several certified reference materials, for example low density fiber blanket and expanded polystyrene board, that can be used to determine the calibration factor in Eq. (1) and that are presented by the National Institute for Science and Technology (NIST) [31]. Since the FOX 603 comes with a database of the calibration factors issued by NIST, based on high density glass fiber board (SRM 1450b), these calibration factors were used in our calculations.

5. Results and discussion

5.1. Regression methods used to calculate thermal properties

5.1.1. Stage-1 steady-state test to determine thermal conductivity

In order to determine the thermal conductivity using linear regression, Eq. (1) must first be converted to its linearized form as follows:

$$\frac{\Delta T}{SE} = \frac{1}{\lambda}\Delta x + 2R_{\text{contact}} \tag{6}$$

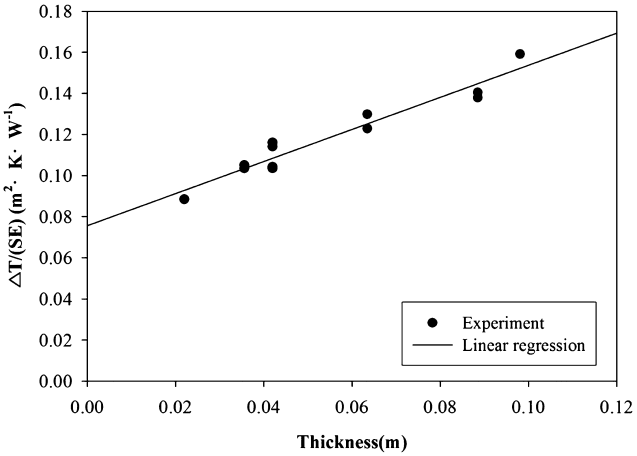

Fig. 3. Scatter plot of the measured data ($\Delta T/SE$) from steady-state heat flux tests as a function of specimen thickness, and the linear regression line plotted over the source data.

The scatter plot of $\Delta T/SE$ against specimen thickness is shown in Fig. 3 and the solid line is the linear regression line obtained from test measurement data. The slope $(1/\lambda)$ is 0.78 $m\,K\,W^{-1}$, corresponding to a thermal conductivity $\lambda = 1.28$ $W\,m^{-1}\,K^{-1}$. Furthermore, the contact resistance is 0.038 $m^2\,K\,W^{-1}$, which is obtained by halving the value of the y-intercept ($2R_{\text{contact}}$) in Fig. 3. The significant effect of the contact resistance, when trying to measure the thermal conductivity of cementitious materials, is strongly supported by the linear regression result in Fig. 3, where the solid regression line is a tight fit with the measured data points.

Some practical considerations include ensuring that output saturation never occurs in the heat flow meter, as this would otherwise limit its capacity to register higher levels of heat flow; minimum specimen thickness is thus defined by the need to avoid saturation of the heat flow meter. The heat flow meters in the Fox 603 machine are capable of detecting up to 20,000 μV, which suggests that at the thermal conductivities measured and a 10 °C temperature difference, the thinnest specimen that can be used is theoretically 10 mm thick. This is because the density of heat flow under steady-state conditions increases with the thinner specimen. Conversely, thicker specimens make it more difficult to prevent perimeter (radial) heat loss through the insulation that surrounds the specimen, due to higher surface area. For this reason, an appropriate range of specimen thicknesses for thermal conductivity testing must be chosen based on the instrument capacity and temperature boundary conditions.

5.1.2. Stage-2 non steady-state test to determine other thermal properties

Once the thermal conductivity and contact resistance are known, Eqs. (3) and (5) can be used to derive the thermal diffusivity and specific heat capacity using a non-steady-state test method. The following expression can be derived from Eqs. (3) and (5):

$$q_{\text{specimen}} = \frac{1}{1/SE - 2R_{\text{contact}}/\Delta T} = \lambda\left\{\frac{\Delta T}{L} + \sum_{n=1}^{\infty}\beta_n\frac{n\pi}{L}\cos\left(\frac{n\pi x}{L}\right)e^{-(n\pi/L)^2 at}\right\} \tag{7}$$

To facilitate non-linear regression analysis, the infinite summation of Eq. (7) must be dealt with in approximate form. Since most insulation materials have lower thermal conductivity than hardened cement paste, the first-order term of the analytical solution is more dominant with thinner samples [32,33]. Since insulation

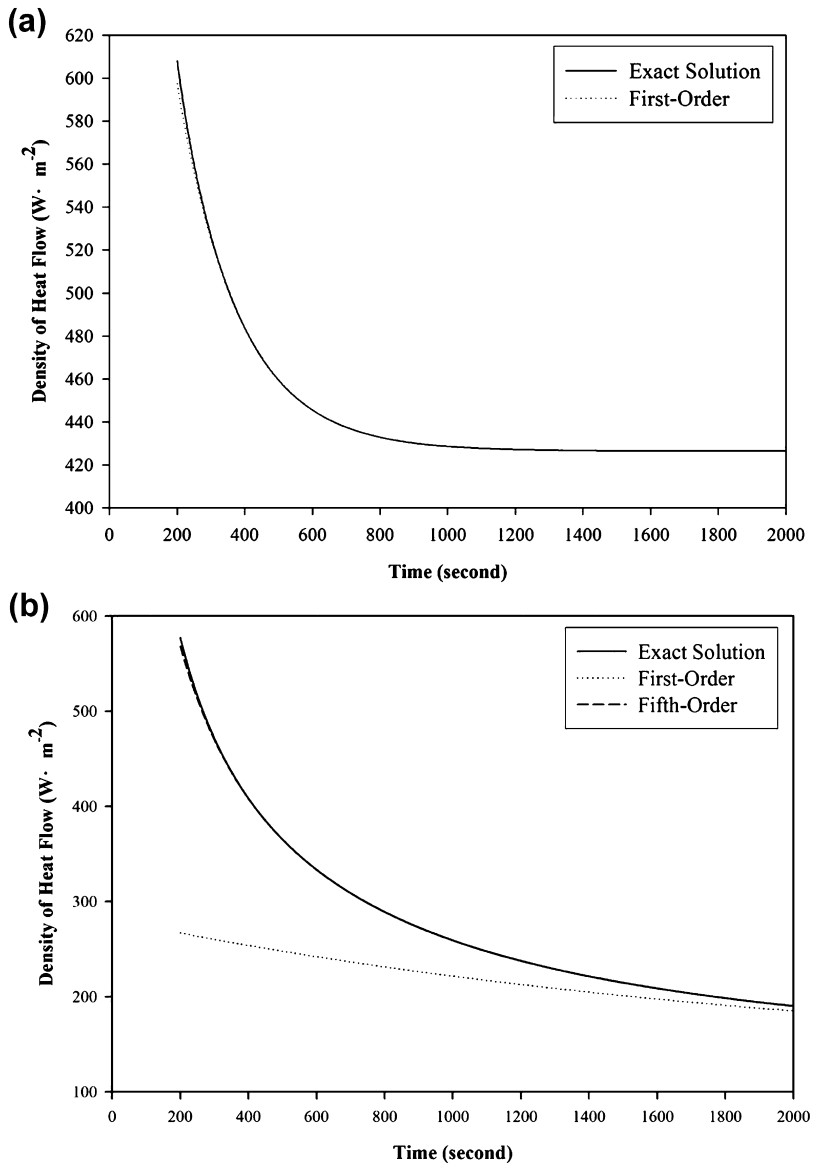

Fig. 4. Theoretical density of heat flow of the benchmark problem as a function of time, solved with different order terms: (a) 30 mm and (b) 100 mm thickness test specimens.

materials possess very low thermal conductivities, 20–30 mm specimen thicknesses are not only enough to measure their thermal properties, but also their contact resistance is negligible due to the high value of the reciprocal of the thermal conductivity in Eq. (1). However, for cementitious materials it is necessary to reconsider the approximation for the summation of whether the first-order term is sufficient to determine the thermal properties from a non-steady-state test. In order to evaluate this approximation, a benchmark problem was solved with the thermal conductivity obtained above and a typical representative value of thermal diffusivity (5×10^{-7} m^2 s^{-1}) for the hydrated cement paste. The results from the benchmark solution are shown in the form of heat flow profiles in Fig. 4. The plots in this figure show the evolution of heat flow over time for the 30 mm and 100 mm thick cement paste specimens that were tested. While for the 30 mm thick specimen in Fig. 4(a) the first-order term dominates over the sum of the remaining terms as heat flow magnitude rapidly approaches the steady state regime, the 100 mm thick sample in Fig. 4(b) requires higher-order terms to be included in order to closely approximate the exact solution. Therefore, for the 100 mm thick hydrated cement paste sample it is necessary to sum up to the fifth-order term in order to approximate the high level of accuracy achieved for the 30 mm case. Although the significance of each term in the equation is reduced, the accuracy to converge to exact values of the heat flow increases with the addition of higher-order terms. As a consequence, calculations of the heat flow equation were added up to the fifth-order terms of Eq. (7) in the present study, to ensure comparable high accuracy of the non-linear regression results obtained.

Fig. 5 shows a typical signal of the heat flow meter during the very early test period. The analytical solution in Fig. 4 shows the reduction in the heat flow over time. However, Fig. 5 shows the increase in the heat flow over a 150 s interval. This is because of the time lag that occurs as heat travels between the heat source and the active heat flow meter, with transient storage of the bulk of this heat (at least initially) occurring in the mass of material forming the sample and equipment. In practice, the actual start-point is arbitrary, since only the relative time is required for non-linear regression. The upper plot in Fig. 6 (upper) shows typical signal data from the heat flow meter when the heat flow reaches the measurable range. Heat flow fluctuations exist and are an artifact of the way

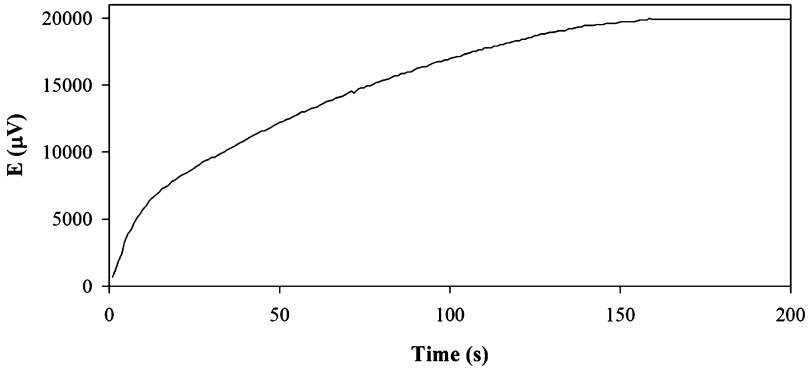

Fig. 5. A typical heat flow meter output signal detected during the first 300 s of testing.

that the heating/cooling elements in the FOX 603 test machine are regulated; in one sense they are analogous to fluid flow fluctuations close to a wall [34]. Accordingly, the general tendency of the heat flow is more important than its local tendency. Non-linear regression analysis of the signal data calls for use of the Newton–Raphson method, and depending on the size of dataset obtained this could consume significant computational resources: i.e., CPU, time, and memory.

When 100 data points are randomly sampled at 6 min intervals, the size of the dataset can be reduced as shown in Fig. 6 (lower) to make the problem manageable. The variation in mean value when this was compared against the full dataset was less than 10 μV, which suggests that the general trend had been preserved. 700 data points, captured 42 min after the start of the measurement, were used for the non-linear regression results reported in the present study.

The basic form of the non-linear regression model is:

$$q_{\text{specimen,i}} = \frac{1}{1/SQ - 2R_{\text{contact}}/\Delta T} = f(t_i, \{\gamma\}) + \varepsilon_i \tag{8}$$

where, $f(t_i,\{\gamma\})$ is the non-linear response function, $\{\gamma\}$ are the parameters released in the regression computation, and ε_i is the residual term. The contact resistance of an individual specimen is recalculated from the mean value of the thermal conductivity obtained from the Stage-1 steady-state tests using Eq. (1). The response function, which is independent of test start time and can be used to evaluate the thermal diffusivity, is obtained from:

$$f(t_i, \{\gamma\}) = \lambda \left[\frac{\Delta T}{L} + \sum_{n=1}^{\infty} \beta_n \frac{n\pi}{L} \cos\left(\frac{n\pi x}{L}\right) \exp\left\{ -\left(\frac{n\pi}{L}\right)^2 \gamma_0 (t_i + \gamma_1) \right\} \right] \tag{9}$$

where, γ_0 corresponds to the thermal diffusivity, and γ_1 is the time lag. Once the initial starting values for the parameters have been assigned and assuming the residuals follow a normal distribution, the parameters are numerically computed using the Newton–Raphson method:

$$\{\gamma\}_{n+1} = \{\gamma\}_n - \left[\frac{\partial^2 \left(\sum_i {\varepsilon_i}^2\right)}{\partial \{\gamma\}^2} \bigg|_{\{\gamma\}=\{\gamma\}_n} \right]^{-1} \cdot \left[\frac{\partial \left(\sum_i {\varepsilon_i}^2\right)}{\partial \{\gamma\}} \bigg|_{\{\gamma\}=\{\gamma\}_n} \right] \tag{10}$$

where, $\{\gamma\}$ is a vector of γ_0 and γ_1, and ε_i is ith component of residuals. In the present study, these computations were done using a computer program that was developed using MATLAB. The non-linear regression model (10) and our response function (9) were successfully applied to the non-steady state data sets. Fig. 7 compares the heat flows through the specimen versus time between the non-linear regression and experimental data. As shown in Fig. 7(a), the density of heat flow for the 35.8 mm specimen rapidly approaches steady state, so that the first-order term correctly describes the experimental measurements. In contrast, the 88.5 mm specimen in Fig. 7(b) slowly approaches steady state, resulting in a mis-match between the first-order term and the experiment during the non-steady-state period. The 35.8 mm

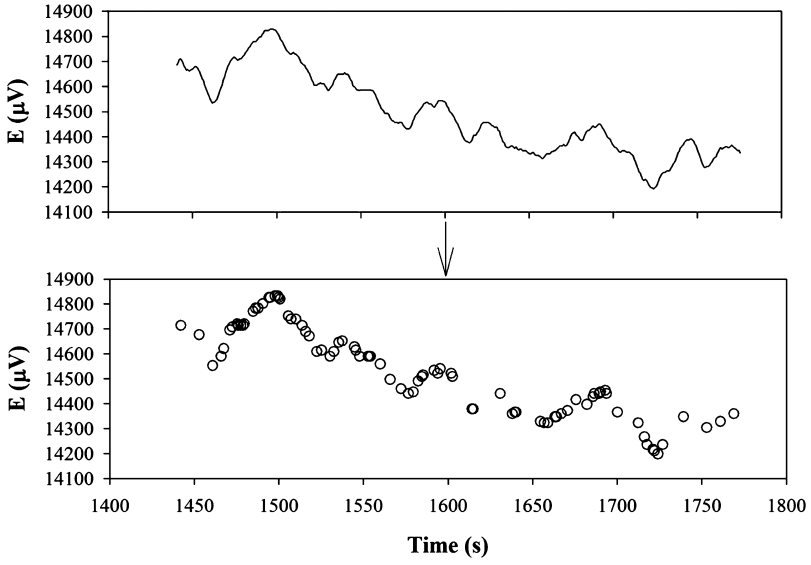

Fig. 6. Comparison of the real-time (upper) versus randomly selected (lower) data from non-steady-state testing.

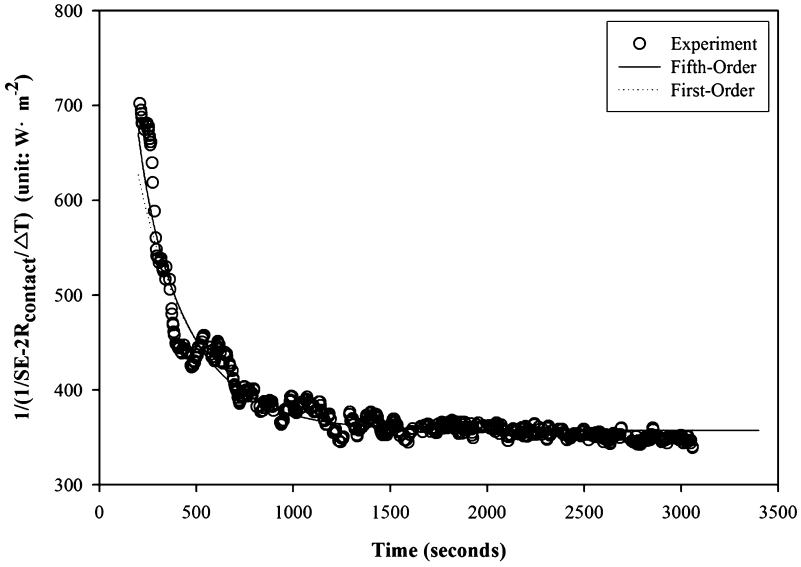

(a)

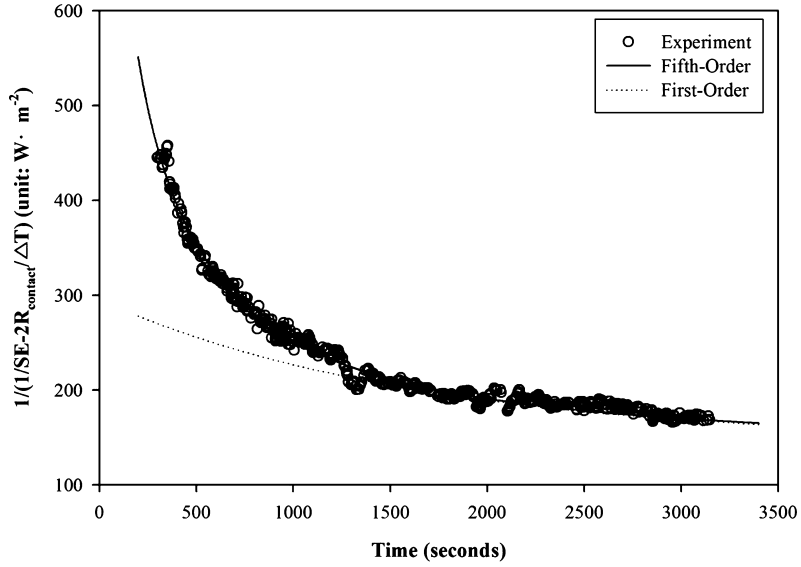

(b)

Fig. 7. Comparative plots of experimental data versus non-linear regression results obtained using up to fifth-order terms with an assumption that residuals follow the normal distribution: (a) 35.8 mm and (b) 88.5 mm thick specimens.

thick specimen shows the expected rapid reduction in the density of heat flow in the non-steady-state and the fluctuation of its signal data is higher than that of the 88.5 mm specimen. This suggests that cementitious materials require a specimen thickness of between 50 and 100 mm and use of the higher-order terms of the analytical solution to calculate their thermal properties.

5.2. Statistical assessment

In order to validate the normal distribution, the most common method is quantile–quantile plot (or Q–Q plot) evaluation. Normal theoretical quantiles are theoretical points of the cumulative normal distribution corresponding to each data point. The basic idea of the Q–Q plot is to compare the cumulative probability of the measured data against that of the assumed distribution, so that, if the points in a Q–Q plot lie roughly on a diagonal line, the assumption is accepted. We first tested the residuals obtained from the non-steady-state test of the 35.8 mm and 88.5 mm specimens in Fig. 8(a) and (b). As the results show, the residuals are characterized by heavy tails in the Q–Q plot, although we see a linear tendency between −1 and 1 theoretical quantiles. Some insight into the reason of the heavy tails is provided from the data in Fig. 7 where part of the (theoretical) solid line is not always well matched to the measured data points. The heavy tails are associated with these early-stage fluctuations, which in turn lead to large residuals. As shown in Fig. 7, these fluctuations mostly occur at an early stage of the non-steady-state test. For this reason, the measured data before 500 s was excluded and the resulting Q–Q plots are reproduced in Fig. 8(c) and (d).

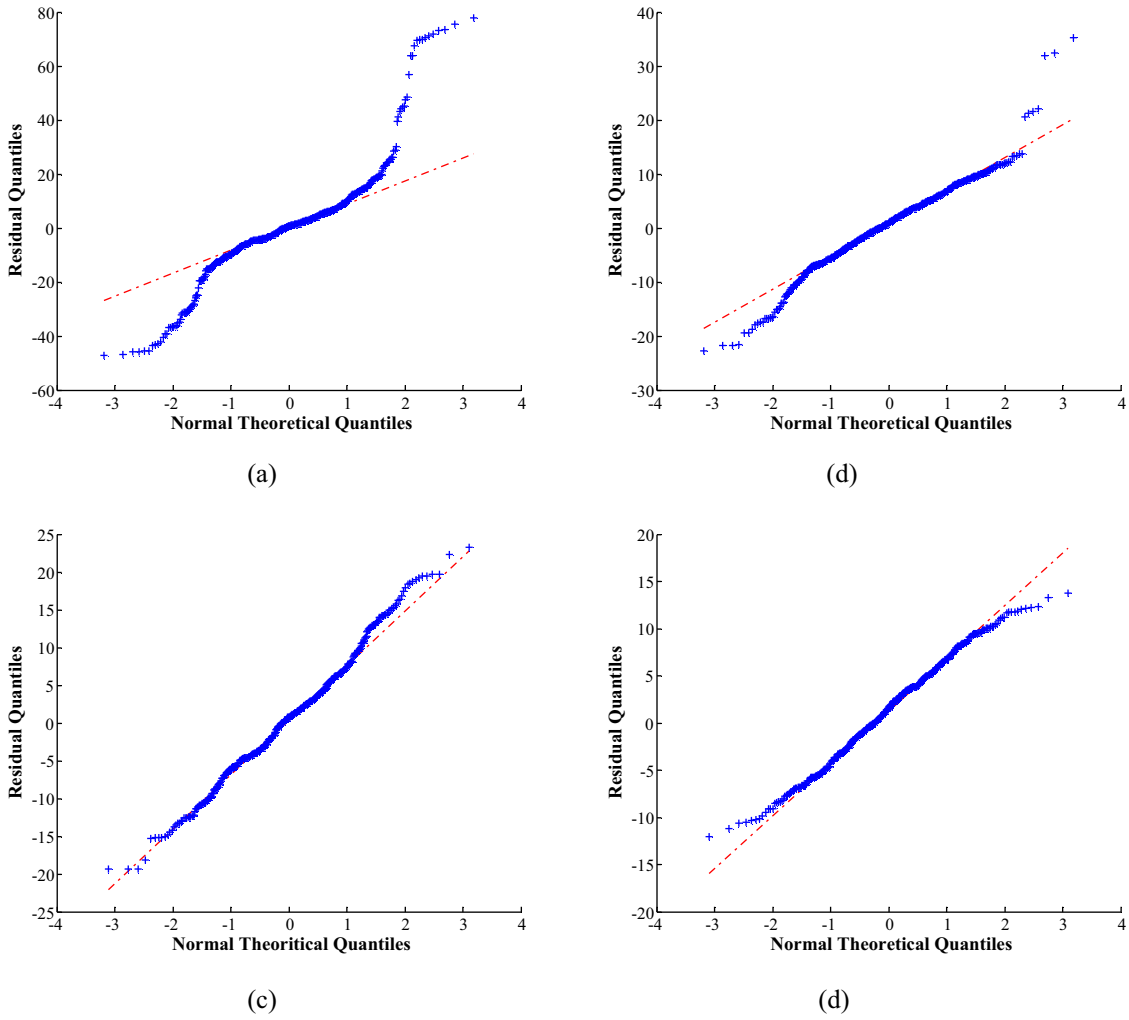

Fig. 8. *Q–Q* plot analysis of residuals: total residuals of (a) 35.8 mm and (b) 88.5 mm test samples, and partial residuals excluding data from the early test period of (c) 35.8 mm and (d) 88.5 mm samples.

These Q–Q plots provide a strong indication that the residuals of the regression analysis follow a normal distribution. The intrinsic thermal mass of the test equipment and how it interacts with the test specimen, laboratory environment and even the people carrying out the test could be a contributing factor for the instability of the heat flow meter readings during the initial period of testing. Accurate values of thermal properties can thus be derived from data that excludes measurements taken during the very early period of testing. The derived thermal diffusivities and heat capacities are listed in Table 2. It is important to note that these values are only applicable within the test temperature range. There is no dependence between thermophyscial properties and the length of the sample. However, the length of the sample affects perimeter heat loss through the insulation surrounding the samples as well as thermal radiation even though the guarded heat flow meter measurement assumes unidirectional heat flow and no thermal radiation. According to the ISO guide [2], the standard and relative uncertainties of the measured thermal properties were determined with 95% level of confidence interval and a normal distribution. The contributory sources of uncertainty for the guarded heat flow meter measurement are thus the thickness of samples, temperature difference, and heat flow meter. Table 3 gives a summary of the results of this analysis. Overall, the relative uncertainties were estimated between 7.7 and 8.9%.

Table 2
Thermal properties of hardened cement pastes with 0.4 w/c ratio derived from nonlinear regression.

Length (mm)	Thermal diffusivity (10^{-7} m^2 s^{-1})	Volumetric specific heat capacity (kJ m^{-3} K)	Specific heat capacity (kJ kg^{-1} K^{-1})
35.8	4.83	2651.5	1.25
63.6	4.66	2747.3	1.30
88.5	4.82	2657.5	1.28

Table 3
Standard and relative uncertainties of thermal properties.

Thermal property	Probability distribution	Standard uncertainty	Relative uncertainty (%)
Thermal conductivity	Normal	0.10 (W m^{-1} K^{-1})	7.7
Thermal diffusivity	Normal	0.39 (10^{-7} m^2 s^{-1})	8.2
Volume specific heat capacity	Normal	237.3 (kJ m^{-3} K^{-1})	8.8
Specific heat capacity	Normal	0.11 (kJ kg^{-1} K^{-1})	8.9

6. Conclusions

Thermal conductivity, thermal diffusivity, volumetric specific heat capacity, and specific heat capacity of hardened cement paste were determined experimentally by the guarded heat flow meter method. The combination of multiple steady state data and linear regression enable to measure and evaluate the thermal conductivity and contact resistance of the hydrated cement paste. Furthermore, a new methodology that combines non-steady-state testing and non-linear regression analysis was proposed to estimate thermal diffusivity, volumetric specific heat capacity, and specific heat capacity simultaneously. From statistical analysis of the residuals obtained from non-linear regression, the research suggests that part of the non-steady state data captured during the early stage of testing needs to be excluded, to eliminate inertial and secondary effects. A thin sample (35.8 mm) shows higher initial fluctuations in the heat flow signal than a thicker (88.5 mm) sample when using the non-steady-state test method. Since the heat flow meter in reality measures an electrical signal, the dramatic reduction in the density of heat flow can generate electrical signal fluctuations. This is attributed to the more rapid approach to steady state of the thin sample, and suggests that there is a range of 'proper' sample thicknesses when carrying out unsteady-state tests of between 50–100 mm for hydrated cement pastes and similar materials. The relative uncertainties, based on ISO guidelines, were comparable to those obtained from ceramics using the laser flash method, which is a non-contact method.

Acknowledgements

The work reported in this publication has been funded through research grant number ENG016 RGG0593, awarded by the Gulf Organization of Research and Development (GORD), Qatar. The authors would also like to express their sincere gratitude to Naomi Patterson and Hoda Beltagui, for their assistance with experimental test preparations. Furthermore, we wish to record our appreciation to John Masson and Douglas (Dougie) Craighead for their support with the initial installation of the FOX 603 test machine.

Appendix A.

The temperature function is divided into two parts as:

$$T(x,t) = u(x,t) + w(x)$$

where, $w(x)$ is independent from time values, and it can be expressed as follows due to boundary conditions:

$$w(x) = \frac{\Delta T}{L^2/\lambda + 2LR_{\text{contact}}}$$

We obtain the series solution for $u(x,t)$ by performing separation of variables as considering as a non-homogeneous partial differential equation:

$$u(x,t) = \sum_{n=1}^{\infty} \left\{ \beta_n \cos(\beta_n x) + \frac{1}{\lambda R_{\text{contact}}} \sin(\beta_n x) \right\} T_n(t) \quad \text{in} \quad x \in (0, L)$$

The eigenvalues β_n is referred as the Sturm–Liouville problem and satisfy the functional relationship:

$$\tan(L\beta_n) = \frac{2\lambda R_{\text{contact}} \beta_n}{(\lambda R_{\text{contact}} \beta_n)^2 - 1}$$

The non-homogeneous equation is expressed as:

$$T_n(t) = e^{-\beta_n^2 at} \left\{ T_n(0) + g_n \int_0^t e^{\beta_n^2 ap} dp \right\}$$

$T_n(0)$ and g_n are determined to satisfy the initial condition as follows:

$$T_n(0) = \frac{\int_0^L (T_0 - w(x)) X_n(x) dx}{\int_0^L X_n(x)^2 dx} \quad \text{and} \quad g_n = \frac{a \int_0^L \frac{\partial^2}{\partial x^2} w(x) X_n(x) dx}{\int_0^L X_n(x)^2 dx} \text{where,}$$

$X_n(x) = \beta_n \cos(\beta_n x) + (1/\lambda R_{\text{contact}}) \sin(\beta_n x)$

This solution can be applied to non-linear regression for the cases that an apparatus provides larger contact resistance and significant temperature discontinuity.

References

[1] A. Bouguerra, A. Ait-Mokhtar, O. Amiri, M. Diop, Measurement of thermal conductivity, thermal diffusivity and heat capacity of highly porous building materials using transient plane source technique, Int. Commun. Heat Mass Transf. 28 (2001) 1065–1078.
[2] R.F. Speyer, Thermal Analysis of Materials, CRC Press, New York, 1994.
[3] D. Bentz, Transient plane source measurements of the thermal properties of hydrating cement pastes, Mater. Struct. 40 (2007) 1073–1080.
[4] A. Bouguerra, J. Laurent, M. Goual, M. Queneudec, The measurement of the thermal conductivity of solid aggregates using the transient plane source technique, J. Phys. D: Appl. Phys. 30 (1997) 2900.
[5] B. Milovanovic, I. Banjad Pecur, I. Gabrijel, Measuring thermal properties of hydrating cement pastes, in: 31st Cement and Concrete Science Conference, Imperial College London, United Kingdom, 2011.
[6] K.H. Kim, S.E. Jeon, J.K. Kim, S. Yang, An experimental study on thermal conductivity of concrete, Cem. Concr. Res. 33 (2003) 363–371.
[7] M. Khan, Factors affecting the thermal properties of concrete and applicability of its prediction models, Build. Environ. 37 (2002) 607–614.
[8] P. Mounanga, A. Khelidj, G. Bastian, Experimental study and modelling approaches for the thermal conductivity evolution of hydrating cement paste, Adv. Cement Res. 16 (2004) 95–103.
[9] R. Demirboğa, R. Gül, The effects of expanded perlite aggregate, silica fume and fly ash on the thermal conductivity of lightweight concrete, Cem. Concr. Res. 33 (2003) 723–727.
[10] P. Duxson, G.C. Lukey, J.S. van Deventer, Thermal conductivity of metakaolin geopolymers used as a first approximation for determining gel interconnectivity, Ind. Eng. Chem. Res. 45 (2006) 7781–7788.
[11] P.A. Fokaides, S.A. Kalogirou, Application of infrared thermography for the determination of the overall heat transfer coefficient (*U*-value) in building envelopes, Appl. Energy 88 (2011) 4358–4365.
[12] C. Martias, Y. Joliff, B. Nait-Ali, J. Rogez, C. Favotto, A new composite based on gypsum matrix and mineral additives: hydration process of the matrix and thermal properties at room temperature, Thermochim. Acta 567 (2013) 15–26.
[13] M. Mantelli, M. Yovanovich, Thermal contact resistance, Spacecraft Therm. Control Handb. 1 (2002).
[14] Y. He, Rapid thermal conductivity measurement with a hot disk sensor: Part 1. Theoretical considerations, Thermochim. Acta 436 (2005) 122–129.
[15] A. Göbel, F. Hemberger, H.-P. Ebert, M. Jansen, J. Wilfert, Thermophysical properties of an amorphous polymer-derived Si/B/N/C ceramic, Thermochim. Acta 520 (2011) 20–24.
[16] H.F.W. Taylor, Cement Chemistry, Thomas Telford, 1997.
[17] Guide to the Expression of Uncertainty in Measurement, International Organization for Standardization, Geneva, Switzerland, 1995.
[20] ASTM C 177, Standard test method for steady-state heat flux measurements and thermal transmission properties by means of the guarded-hot-plate apparatus, American Society for Testing and Materials and Structures.
[21] ASTM C 518-10, Standard test method for steady-state thermal transmission properties by means of the heat flow meter apparatus, American Society for Testing and Materials and Structures.
[22] ASTM C 1044, Standard practice for using a guarded-hot-plate apparatus or thin-heater apparatus in the single-sided mode, American Society for Testing and Materials and Structures.
[23] M.H. Rausch, K. Krzeminski, A. Leipertz, A.P. Fröba, A new guarded parallel-plate instrument for the measurement of the thermal conductivity of fluids and solids, Int. J. Heat Mass Transf. 58 (2013) 610–618.
[24] E. Kamseu, B. Nait-Ali, M. Bignozzi, C. Leonelli, S. Rossignol, D. Smith, Bulk composition and microstructure dependence of effective thermal conductivity of porous inorganic polymer cements, J. Eur. Ceram. Soc. 32 (2012) 1593–1603.
[25] A. Brzezinski, A. Tleoubaev, Effects of interface resistance on measurements of thermal conductivity of composites and polymers, in: Proceedings of the 30th Annual Conference on Thermal Analysis and Applications (NATAS), B&K Publishing, 2002, pp. 512–517.
[26] A. Tleoubaev, A. Brzezinski, Combined guarded-hot-plate and heat flow meter method for absolute thermal conductivity tests excluding thermal contact resistance, in: Thermal Conductivity 27/Thermal Expansion 15 Conference, 2005.
[27] S.J. Farlow, Partial Differential Equations for Scientists and Engineers, Wiley International Edition, 2012.
[28] P.K. Mehta, P.J.M. Monteiro, Concrete: Microstructure, Properties and Materials, McGraw-Hill, New Jersey, 2006.

[29] L. Czarnecki, A. Garbacz, J. Kurach, On the characterization of polymer concrete fracture surface, Cem. Concr. Compos. 23 (2001) 399–409.
[30] A. Garbacz, L. Courard, K. Kostana, Characterization of concrete surface roughness and its relation to adhesion in repair systems, Mater. Charact. 56 (2006) 281–289.
[31] D. Salmon, Thermal conductivity of insulations using guarded hot plates, including recent developments and sources of reference materials, Meas. Sci. Technol. 12 (2001) R89.
[32] A. Tleoubaev, A. Brzezinski, Thermal diffusivity and volumetric specific heat measurements using heat flow meter instruments, in: Thermal Conductivity 29/Thermal Expansion 17 Conference, 2007.
[33] A.N. Tikhonov, A.N. Tihonov, A.A. Samarskiĭ, Equations of Mathematical Physics, Courier Dover Publications, New York, 1963.
[34] T. Astarita, G.M. Carlomagno, Heat flux sensors, in: Infrared Thermography for Thermo-fluid-Dynamics, Springer, 2013, pp. 49–82.